Textures and Microstructures, Vol. 30, pp. 247–263
Reprints available directly from the publisher
Photocopying permitted by license only

OXIDATION OF ZIRCONIUM ALLOYS. CRYSTALLOGRAPHIC TEXTURE OF ZIRCONIA: INTERPRETATION AND MECHANICAL CONSEQUENCES

M. PARISE, I. TOUET and O. SICARDY *

CEREM-DEM, CEA-Grenoble, 17, rue des Martyrs, 38054 Grenoble Cedex 9, France

(Received 15 December 1997)

In order to have a better knowledge of the mechanical behaviour of the oxide layers growing on zirconium alloys in pressurized water reactors, the textures of different zirconium alloys and their oxide layers are studied. The results show that the texture of the oxide layers present a feature common to all the layers: the tilt angle of the maximum intensities of the pole figures obtained on the layers is almost quite identical for all the studied substrates. The azimuthal reinforcements depend on the metallurgical state of the substrate.

The crystallographic direction of monoclinic zirconia common to all the oxide grains is identified. A computation based on mechanical issues is presented: considering the anisotropic elastic properties of the monoclinic monocrystal, it is shown that the particular crystallographic direction is linked to an isotropic state of strains in the plane of the metal–oxide interface.

Keywords: Zirconium alloys; Oxide growth; Texture analysis; Elastic moduli; Stress computation

0 INTRODUCTION

Zirconium alloys are used as fuel cladding materials in the Pressurized Water Reactors (PWR). On the waterside, the coolant leads to the formation of an oxide layer, whose thickness grows with the time of stay

* Corresponding author.

in the reactor. For Zircaloy-4 type alloys, during uniform corrosion in water at PWR temperature, two different kinetics can be distinguished: first, for thin oxide layers, the thickness grows approximately as cube root of time, afterwards the growth is approximately linear. The change in kinetics occurs for an oxide thickness called transition thickness which is about 2 μm. This phenomenon is known as "breakaway oxidation", following Bradhurst and Heuer (Bradhurst and Heuer, 1970).

Because of the elevated value of the Pilling and Bedworth ratio (Pilling and Bedworth, 1923), the zirconia layers undergo great mechanical stresses. These are, as a first approach, essentially compressive stresses on planes perpendicular to the metal–oxide interface. Mechanical stresses could be responsible for the kinetics transition, through the occurrence of cracks in the oxide layer (Bradhurst, 1970). During the pre-transition step, stresses could also lead to the particular kinetics (Evans *et al.*, 1978). The study of the stresses and strains, either experimentally or through modelling, needs the knowledge of the behaviour of both the metal and the oxide. The Young modulus and the Poisson ratio can be computed for a given direction, with the values of stiffness and compliance moduli (C_{ij} and S_{ij} respectively) listed by Nevitt *et al.* (1988). The values are very different from one direction to another: Young modulus ranges from 122 to 326 GPa and Poisson ratio from 0.13 to 0.43. Monocrystalline monoclinic zirconia has thus very anisotropic elastic properties. Therefore, the study of the crystallographic textures of the oxide layers becomes of special interest.

X-rays diffraction analysis of zirconia layers shows that the layers are mainly composed of the monoclinic form and that the intensity of certain poles, such as $(\bar{1}02)$, are particularly high in comparison with the diffraction diagram of the powder (David *et al.*, 1971). We noticed the same on oxide layers whose thicknesses range from 0.1 to 10 μm. These results point out that in the oxide layers, the monoclinic zirconia has crystallographic directions of growth which seem to be independent of the oxide thickness.

The aim of this article is to specify the orientation of the monoclinic grains in the oxide layers, through the determination of the crystalline textures. This study attempts to find whether the textures of the oxide layers are related to the alloy nature (composition and metallurgical state), to the oxidation kinetics (pre- or post-transition kinetics), or to oxidizing conditions.

1 EXPERIMENTAL

1.1 Samples Preparation

Two types of samples are studied in this work. The first type is cut from Zircaloy-4 alloy sheets, 0.6 mm thick, which are used as spacing grids in PWR. The other type is cut from nuclear fuel cladding of different industrial zirconium-based alloys. The chemical composition and final heat treatment of these different materials are presented in Table I. The grain size ranges from 1 μm for the beta quenched tube to 5 μm for the fully annealed.

The oxide layers studied in this work have very different thicknesses, some being about 500 nm thick, the other about 10 μm. The preparation of the metal before oxidation and the oxidizing conditions will thus be different, depending on whether the oxide layers on these samples will be thin or thick.

1.1.1 Samples Preparation for Thin Oxide Layers

The thicknesses in this range (lower than 500 nm) have to be measured by an optical method, therefore all the samples are polished before oxidation. Sheets are cut by laser into 25 mm diameter samples, and polished on one side only. Tube samples 25 mm long are mounted in a Presi-KMR resin in order to be polished tangentially to the tube axis. The so-obtained surface is a 3 mm × 25 mm rectangle (Fig. 1). The polishing is processed mechanically on SiC papers and finished mechano-chemically with Presi-SPR solution on Supra disks.

TABLE I Metallurgical state and chemical composition (weight percentages)

Sample	*Metallurgical state*	*Shape*	*Sn* %	*Fe* %	*Cr* %	*Nb* %	*V* %	*O* %
Zircaloy-4	Fully annealed	Sheet	1.45	0.2	0.1			0.12
	Stress relieved	Tube						
Low tin content	Stress relieved	Tube						
alloy	Fully annealed	Tube	1.3	0.2	0.1			0.1
	β quenched	Tube						
Very low tin content alloy	Stress relieved	Tube	0.5	0.2	0.1			0.1
Niobium alloy	Fully annealed	Tube				1		0.12
Vanadium alloy	Fully annealed	Tube	0.5	0.6			0.3	0.1

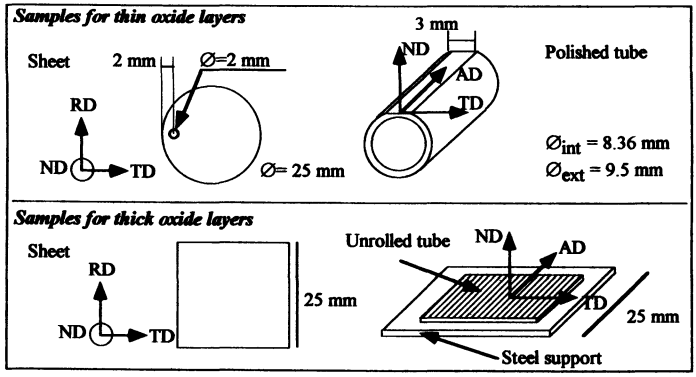

FIGURE 1 Geometry and size of the tube and sheet samples.

1.1.2 Samples Preparation for Thick Oxide Layers

The sheet samples are chemically etched and rinsed. The tube samples are 50 mm long cylindrical sections, made thinner by machine finishing down to a thickness about 0.1 mm. They are then unrolled and point welded to a steel support.

1.2 Oxidizing Conditions and Thickness Measurements

1.2.1 Thin Oxide Layers

The samples are oxidized in a 0.13 l static autoclave partially filled with "PWR solution". This solution, obtained by dissolving 2 ppm of lithium as lithia (LiOH) and 1000 ppm of boron as boric acid (H_3BO_3) in one litre of distilled water, is used to reproduce the chemical conditions in PWRs. The autoclave is heated in a furnace up to 340°C. The volume of solution introduced into the autoclave is chosen so as to attain the liquid/vapour equilibrium; the pressure is then about 15 MPa. The corrosion lasts about 15 days to obtain 500 nm thick layers. Oxide thicknesses are measured by spectrophotometry. (Parise, M., 1996)

1.2.2 Thick Oxide Layers

The unrolled metal samples are oxidized at 400°C, in steam, at a pressure of 10.3 MPa. The thicknesses are estimated by SEM on sections micrographies and weight gain with good agreement.

1.3 Conditions of Pole Figures Measurements

The textures are studied by pole figures (PF). The planes studied are (002)Zr for the different zirconium alloy substrates and $(\bar{1}11)_{\text{monoclinic}}$ and $(111)_{\text{monoclinic}}$ for the zirconia layers. The texture goniometer used in this work is a Huber 4 circles Euler cradle with a 3 kW Inel generator, using the K_α radiation of copper. Two slits are disposed on the side of the counter, the width of which is 3 mm for all the measurements and the aperture depends on the Bragg angle of the PF. This value is 5.5 mm for $(002)_{Zr}$ PF and 6 mm for $(\bar{1}11)_{\text{monoclinic } ZrO_2}$ PF. All the measurements are limited to a tilt angle of 75°. Therefore, no further calculation will be made to take into account the defocalization effects. The detection is achieved by a scintillator counter with a curved graphite monochromator. The background is measured out of Bragg's conditions for the azimuth zero and for all the tilt angles. The angle steps are 2.5° and 5° for the tilt and azimuth angles, respectively; step scan is used and a measure for one (ϕ, χ) position lasts 5 s.

The pole figures are normalized according to:

$$I_{\text{normalized}}(\chi, \phi) = \frac{I_{\text{measured}}(\chi, \phi)}{\int_{\chi=0}^{\chi=75°} \int_{\phi=0}^{\phi=2\pi} I_{\text{measured}}(\chi, \phi) \sin \chi \, d\phi \, d\chi}. \quad (1)$$

The samples are disposed on the goniometer so as to have the rolling or axial axis (for sheets and tubes respectively) parallel to the vertical direction of the pole figures.

1.4 Results

1.4.1 Texture of the Metal

The (002) PFs of α-zirconium are presented in Fig. 2. The texture of zirconium alloys cladding and sheets are strongly marked, since the maximum density is generally about 5. The (002) pole figure of the sheet presents two portions of crown symmetrical to the (ND, TD) plane, with a main tilt of 10°. The (002) PF of the stress relieved tube presents two main intense peaks, which stand on both sides of the (ND, AD) plane. The (002) PF of the stress relieved alloy is dissymmetrical according to (ND, TD) plane; this is due to the pilgrim's step process undergone by the tubes during their manufacturing. The pole figures of

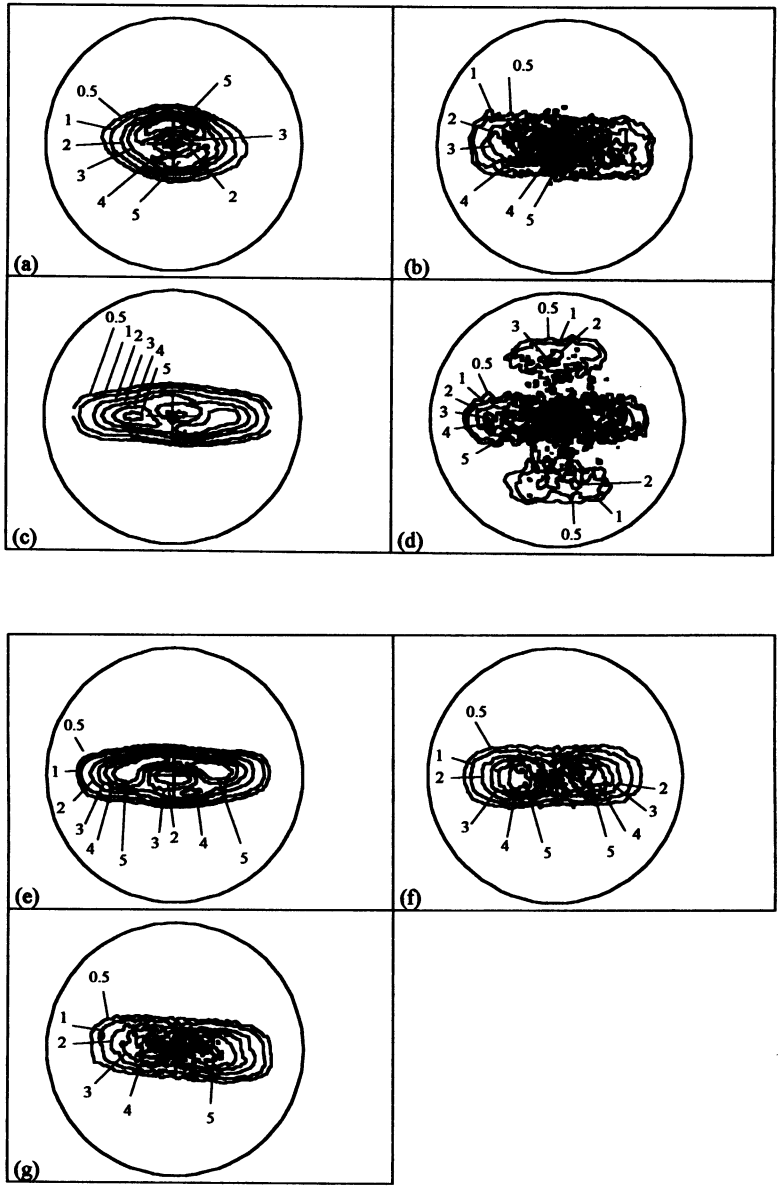

FIGURE 2 (002)Zr pole figures of Zircaloy-4 fully annealed sheet (a), fully annealed low tin content tube (b), stress relieved low tin content tube (c), beta quenched low tin content tube (d), stress relieved very low tin content tube (e), fully annealed niobium alloy tube (f) and fully annealed vanadium alloy tube (g).

the fully annealed and beta quenched alloys both present reinforced intensities in the (ND, TD) plane.

Pole figures obtained for the very low tin content alloy, niobium or vanadium alloys are quite similar to those previously described. The composition changes do not modify the general aspect of the pole figures, which depends only on the metallurgical state. That means that the very low tin content alloy has the same texture as the low tin content alloy in the stress relieved state, and both niobium and vanadium alloys have the same texture as low tin content alloy in the fully annealed state.

With metallurgical states of the metal being the same, the PF obtained on unrolled tubes (Baron *et al.*, 1990) does not present any obvious difference with those obtained on tubes prepared by polishing a plane surface. An example is given for the low tin content, stress relieved alloy in Fig. 3.

This similarity shows that the pole figures of the alloys of this study are independent of the way the tubes have been prepared before oxidation. They depend only on the metallurgical state.

1.4.2 Texture of the Oxide Layers

We specify that we will use for monoclinic zirconia the indices quoted in the 36-420 card of JC-PDS file, even though this one has been replaced by the more recent 37-1484 card: this is in order to remain coherent with the usual indices for this structure.

The oxide layer grown on the sheet exhibits a fibre texture (Fig. 4). The maximum density of the ($\bar{1}11$) pole figure appears for a tilt angle of

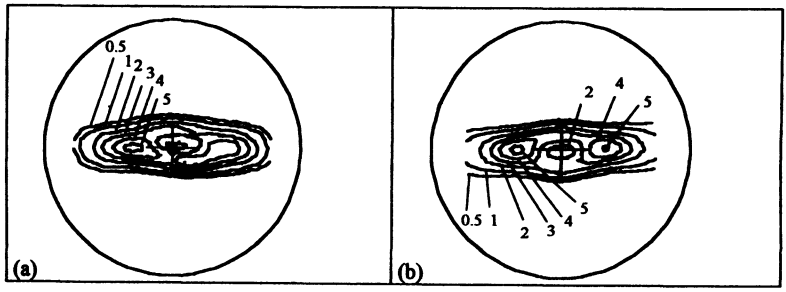

FIGURE 3 (002)Zr pole figures of low tin content alloys on polished tube (a) and unrolled tube (b).

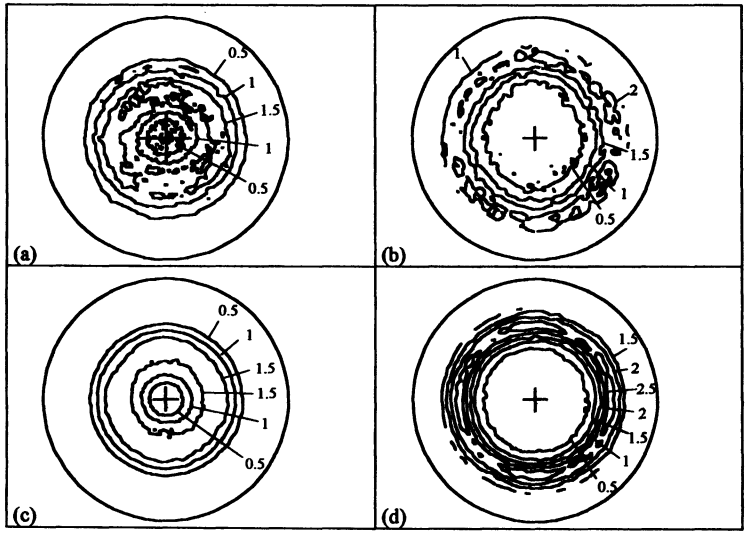

FIGURE 4 ($\bar{1}11$) pole figures of the monoclinic zirconia on 500 nm (a) and 14 μm (c) thick films and corresponding (111) pole figures (b) and (d).

50° in the thin film and 44°for the thick film, with no preferential azimuth and is between 1.5 and 2. For the (111) pole figures the tilt angle is 67° on thin film, 64° on thick film and the density is higher since it is 2.5.

The maximum density in the ($\bar{1}11$) PF obtained for the oxide layers grown on the low tin content alloys tubes in stress relieved state appears for the same tilt angle of 50° as on the sheet but with preferential azimuths around 35° according to the (ND, TD) plane (Fig. 5). The azimuthal reinforcements are dissymmetrical according to this plane. This may be related to the dissymmetry which exists in the (002) pole figure of the base metal. The texture is more strongly marked on the thin layer than on the thick layer since the density is between 2.5 and 3 for the thin layer and is between 2 and 2.5 on the thick layer. Anyway the main feature of the texture, i.e. the tilt angle, does not depend on the oxide thickness.

The ($\bar{1}11$) pole figures obtained for the thin oxide layers grown on the other alloys are presented in Fig. 6. The same main tilt angle as for the layers on the fully annealed sheet or on the low tin content stress relieved tube can be noticed.

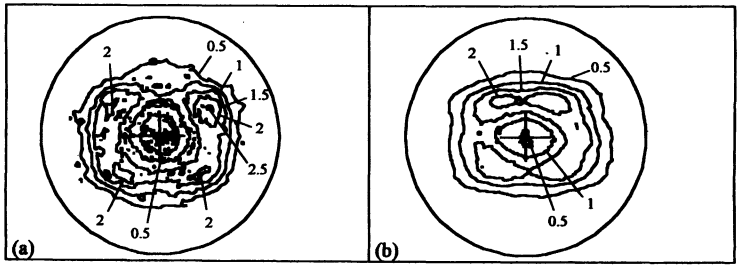

FIGURE 5 ($\bar{1}11$) pole figures of the monoclinic zirconia of 500 nm (a) and 10 μm (b) thick films on stress relieved tubes.

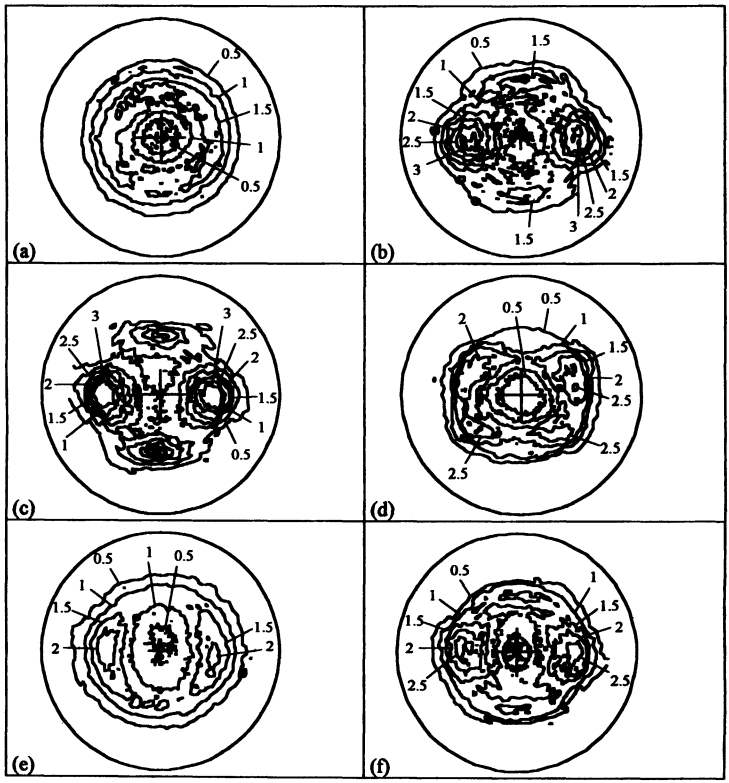

FIGURE 6 ($\bar{1}11$) pole figures of the monoclinic zirconia in 500 nm thick layers grown on sheet (a), fully annealed low tin content tube (b), beta quenched low tin content tube (c), very low tin content stress relieved alloy tube (d), fully annealed niobium alloy tube (e) and fully annealed vanadium alloy tube (f).

The four preferential azimuths are different for the stress relieved tube on one hand and for the fully annealed and beta quenched tube on the other hand. The maxima of the PFs are in the (ND, AD) and (ND, TD) planes (approximately at azimuth 0°, ± 90°, 180°) for layers grown on fully annealed and beta quenched tubes. On the stress relieved tube, we have seen that maxima are at azimuths ± 35° according to (ND, TD) plane. These maxima correspond to densities between 2.5 and 3. The oxide layers grown on the very low tin content alloy, niobium or vanadium alloys, lead to the same pole figures as layers grown on the low tin content alloys, that is to say with preferential azimuths depending on the metallurgical state of the substrate and tilt angle being always about 50°.

According to these different results, the texture of the oxide layers seems to be independent of the metal texture, at least as far as the tilt angle of the maximum intensities is concerned. The ($\bar{1}11$) PF of the oxide layers are thus described by a tilt angle of about 50° common to all the layers grown on the different substrates (sheet or tubes with various heat treatments) at different thicknesses (pre- or post-transition stages).

2 DISCUSSION

2.1 Research of the Fibre Axis

The experimental results show that ($\bar{1}11$) and (111) planes of the monoclinic zirconia are mainly tilted with approximately always the same angle according to the normal to the metal–oxide interface, ranging from 44° to 52° for ($\bar{1}11$) planes and from 64° to 67° for (111) planes. The following calculation aims at showing that this tilt angle corresponds to the fact that the zirconia grows so as to have always the same crystallographic direction perpendicular to the metal–oxide interface. It will be performed according to the reference frame P(OX, OY, OZ) presented in Fig. 7. This reference frame is called "crystallophysic frame", following that proposed by Sirotine and Chaskolskaia (1984), in opposition to the "crystallographic frame", G(Ox, Oy, Oz) which is not an orthonormal one because of the structure of the monoclinic unit cell. The tensors describing the crystal

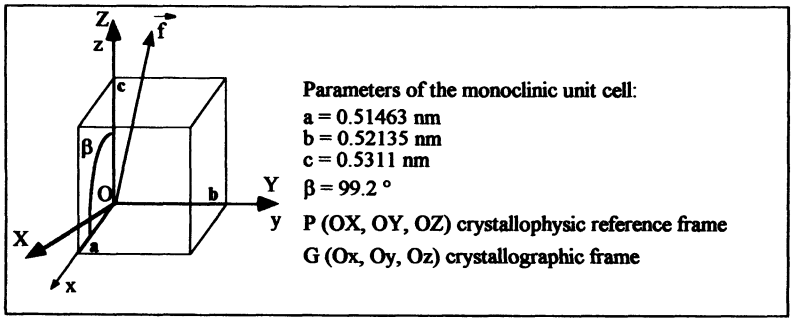

FIGURE 7 Description of the monoclinic unit cell and the reference frame used in the calculations.

properties are expressed in this reference frame, adopted by international conventions for the monoclinic structure.

Let **f** be the unit vector of the direction common to the monocrystals of zirconia, representing the fibre axis. The scalar products of the vector **f**, and the vectors normal to (*hkl*) planes of the (*hkl*) PFs previously studied, $\mathbf{n}_{hkl}$, are equal to the cosine of the tilt angles of the maximum intensities in the PFs, therefore

$$\mathbf{n}_{\bar{1}11} \cdot \mathbf{f} = \cos(50°), \tag{2}$$

$$\mathbf{n}_{111} \cdot \mathbf{f} = \cos(67°). \tag{3}$$

In order to determine the three coordinates f_X, f_Y, f_Z of **f**, a third equation is necessary, which can be simply given by

$$f_X^2 + f_Y^2 + f_Z^2 = 1. \tag{4}$$

Solving the Eqs. (2)–(4), two solutions come:

$$\begin{bmatrix} f_X \\ f_Y \\ f_Z \end{bmatrix} = \begin{bmatrix} -0.167 \\ -0.052 \\ 0.985 \end{bmatrix} \quad \text{and} \quad \begin{bmatrix} f'_X \\ f'_Y \\ f'_Z \end{bmatrix} = \begin{bmatrix} -0.167 \\ 0.984 \\ -0.070 \end{bmatrix}.$$

The choice between these two solutions can be made by pointing out that only the first solution is approximately parallel to the normal to ($\bar{1}02$) plane. Indeed this latter mainly lies parallel to the metal–oxide interface.

If the same calculation is achieved for tilt angles of 44° and 64° for $(\bar{1}11)$ and (111) planes respectively, the solution is

$$\begin{bmatrix} f_X \\ f_Y \\ f_Z \end{bmatrix} = \begin{bmatrix} -0.186 \\ 0.062 \\ 0.981 \end{bmatrix}.$$

The angular shift between these two solutions is 6°. Thus they can be considered as similar.

In order to situate the growth direction of zirconia, a few examples of angles between **f** and some crystallographic directions or vectors normal to simple planes of monoclinic ZrO_2 are listed below:

normal to (100)	100°
normal to (010)	93°
[010] direction	93°
normal to (001)	19°
[001] direction	10°
normal to $(\bar{1}02)$	11°

The **f** direction is thus nearly perpendicular to the binary axis [010] and is very close to [001] direction and to the normal to $(\bar{1}02)$ planes.

2.2 Mechanical Interpretation of the Growth Direction

The texture analysis previously achieved allows us to say that, within about a few degrees, the **f** direction depends neither on the oxide thickness, nor on the alloy nature (only the azimuthal distribution around this direction varies). The question arises of the physical origin of this direction and the interpretation which we propose below is a mechanical one.

The following computation aims at studying the evolution of the stress and strain tensors of a monocrystal according to its orientation in the layer and at looking if the **f** direction does not present some particularities which would favour its selection.

In this section, the mechanical state of a monocrystalline oxide layer is determined for any orientation of the monocrystal with respect to the metallic substrate. This comes down to determine 12 unknown factors, namely the six components of the strain tensor and six of the stress

tensor. Using the matrix form, the strain and the stress tensors are written as

$$\begin{bmatrix} e_1 & e_6/2 & e_5/2 \\ e_6/2 & e_2 & e_4/2 \\ e_5/2 & e_4/2 & e_3 \end{bmatrix} \quad \text{and} \quad \begin{bmatrix} \sigma_1 & \sigma_6 & \sigma_5 \\ \sigma_6 & \sigma_2 & \sigma_4 \\ \sigma_5 & \sigma_4 & \sigma_3 \end{bmatrix},$$

respectively.

In order to use the index $i=1,\ldots,6$ the crystallophysic frame is named (Ox_1, Ox_2, Ox_3) and not P(OX, OY, OZ) in this section.

Since the oxide layer is considered as an elastic material, the Hooke's law applies and gives six equations:

$$\sigma_i = \sum_{j=1}^{j=6} C_{ij}.e_j, \quad i = 1,\ldots,6 \tag{5}$$

with

$$[C_{ij}] = \begin{bmatrix} 358 & 144 & 67 & 0 & -25.9 & 0 \\ 144 & 426 & 127 & 0 & 38.3 & 0 \\ 67 & 127 & 240 & 0 & -23.3 & 0 \\ 0 & 0 & 0 & 99.1 & 0 & -38.8 \\ -25.9 & 38.3 & -23.3 & 0 & 78.7 & 0 \\ 0 & 0 & 0 & -38.8 & 0 & 130 \end{bmatrix} \text{(GPa)}$$

according to Nevitt *et al.* (1988). The other required equations are provided by two hypotheses physically plausible on the state of the monocrystalline layer. Let **q** be the vector normal to the metal–oxide interface.

First hypothesis (*usually used in the case of thin layers*) Stresses on any plane parallel to the free surface (thus normal to **q**) equal zero. This leads to the matrix relation:

$$\begin{bmatrix} \sigma_1 & \sigma_6 & \sigma_5 \\ \sigma_6 & \sigma_2 & \sigma_4 \\ \sigma_5 & \sigma_4 & \sigma_3 \end{bmatrix} \begin{pmatrix} q_1 \\ q_3 \\ q_3 \end{pmatrix} = \begin{pmatrix} 0 \\ 0 \\ 0 \end{pmatrix}. \tag{6}$$

Second hypothesis Any plane parallel to the metal–oxide interface is strained parallel to itself. In other words, the strained vector

of **q** is collinear to **q**, which leads to:

$$\begin{bmatrix} e_1 & e_6/2 & e_5/2 \\ e_6/2 & e_2 & e_4/2 \\ e_5/2 & e_4/2 & e_3 \end{bmatrix} \begin{pmatrix} q_1 \\ q_2 \\ q_3 \end{pmatrix} = \lambda \begin{pmatrix} q_1 \\ q_2 \\ q_3 \end{pmatrix}, \ \lambda \text{ being real.} \qquad (7)$$

For each orientation of the monocrystal with respect to the metal–oxide interface, the coordinates of **q** can be expressed in the crystallophysic frame as a function of the crystallographic parameters a, b, c and β of the monoclinic unit cell.

The relations (5)–(7) form together a linear system of 12 equations and 12 unknowns with λ as a parameter. Stresses and strains of the monocrystalline layer can then be determined to within a proportional factor λ, for any orientation of **q**. In order to solve the system, the value of λ has to be fixed for each orientation of **q**, for example so as to have a surfacic dilatation equal to -1%. The computation is first achieved in the crystallophysic frame but the strain and stress tensors can be expressed in their own principal frames.

The analysis of all the solutions shows that not all the crystallophysic directions can lead to a physically realistic result. For example, if the computation is made for **q** being normal to (011) plane, the values of the strains and stresses tensors in the principal frames of strains and stresses are, respectively,

$$\begin{bmatrix} -1.526 & 0 & 0 \\ 0 & 0.526 & 0 \\ 0 & 0 & 0.205 \end{bmatrix} \text{(in \%)} \quad \text{and} \quad \begin{bmatrix} -4.87 & 0 & 0 \\ 0 & 0.35 & 0 \\ 0 & 0 & 0 \end{bmatrix} \text{(in GPa).}$$

A characteristic feature in this case is that the values of the principal stresses are very different. This leads to very important shear stresses on planes perpendicular to the metal–oxide interface. The second principal stress has a positive value, thus is a tensile stress, which is very unlikely considering the experimental compressive stresses mentioned in the literature (Bradhurst and Heuer 1970; Roy and Burgess, 1970).

If the previous computation is achieved now for **q** being the axis of the fibre texture identified in the experimental part, the strains and stresses tensors expressed in the principal frame of the strains (Oy_1,

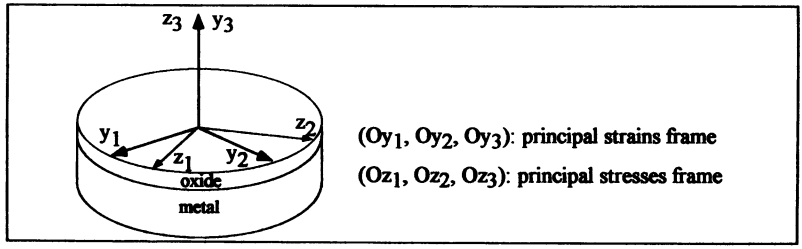

FIGURE 8 Principal strains and stresses frames.

Oy_2, Oy_3) and stresses (Oz_1, Oz_2, Oz_3) (Fig. 8), they are respectively expressed as

$$\begin{bmatrix} -0.539 & 0 & 0 \\ 0 & -0.461 & 0 \\ 0 & 0 & 0.362 \end{bmatrix} \text{(in \%) and } \begin{bmatrix} -2.49 & 0 & 0 \\ 0 & -2.17 & 0 \\ 0 & 0 & 0 \end{bmatrix} \text{(in GPa).}$$

In this case, all the stresses are compressive ones. In addition to that, the two principal strains (respectively stresses) in the (Oy_1, Oy_2) plane (respectively (Oz_1, Oz_2)) are close to one another, expressing an isotropic mechanical state in the plane of the metal–oxide interface.

If a condition of isotropic strain in the plane of the interface is added to the previous system of equations, the computation leads to only four solutions, which are:

Solution	q_1	q_2	q_3
1	−0.185	0	0.983
2	0.714	0	0.700
3	0.567	±0.627	0.534
4	0.910	±0.038	−0.416

One points out that the first solution is very close to the **f** direction, the angular shift between these two vectors being 3°. One can summarize the previous computation saying that the **f** direction is, from a mechanical point of view, consistent with a planar state of stresses and an isotropic state of strains in the plane of the metal–oxide interface. For a highly anisotropic monocrystal such as monoclinic zirconia, only few crystallographic directions verify this property.

3 CONCLUSION

The oxide grown on waterside zirconium alloys fuel claddings exhibits marked crystallographic textures. This study shows that zirconia grains have a common crystallographic direction **f** which is mainly normal to the metal–oxide interface. The whole textures features do not depend on the layer thickness in the range from 0.1 to 10 μm; one can conclude that there is no textures transition at the kinetics transition of oxide layer growth.

The **f** direction depend neither on the alloy composition nor on its metallurgical state: only the azimuthal distribution of oxide crystallites around this direction varies. In the case of Zircaloy-4 fully annealed sheet, there is no azimuthal reinforcements so one has to deal with fibre texture. In the case of tubes of various compositions and metallurgical states, one observes azimuthal reinforcements linked to the final heat treatment of the metal.

From a mechanical point of view, the common **f** direction presents the particular feature to allow an isotropic state of strains in the plane of the metal–oxide interface, in spite of the highly anisotropic elastical properties of monoclinic zirconia. A further interesting development of this mechanical approach would be to explain and take into account the differences in azimuthal distributions between sheets and tubes in the various metallurgical states previously described.

Acknowledgements

The authors want to thank Framatome and Electricite de France for financial support and providing materials.

References

Baron, J.L., Esling, C., Feron, J.L., Gex, D., Glimois, J.L., Guillen, R. *et al.* (1990). Interlaboratories tests of textures of Zircaloy-4 tubes. Part 1: pole figure measurements and calculation of Kearns coefficients. *Texture and Microstructures*, **12**, 125–140.

Bradhurst, D.H. and Heuer, P.M. (1970). The influence of oxide stress on the breakaway oxidation of Zircaloy-2, *Journal of Nuclear Materials*, **37**, 35–47.

David, G., Geschier, R. and Roy, C. (1971). Etude de la croissance de l'oxyde sur le zirconium et le Zircaloy-2. *Journal of Nuclear Materials*, **38**, 329–339.

Evans, H.E., Norfolk, D.J. and Swan, T. (1978). Perturbation of parabolic kinetics resulting from the accumulation of stresses in protective oxide layers. *Journal of the Electrochemical Society*, **125**(7), 1180–1185.

Nevitt, M.V., Chan, S.K., Liu, J.Z., Grimsditch, M.H. and Fang, Y. (1988) The elastic properties of monoclinic ZrO_2. *Physica B*, **150**(1,2), 230–233.

Parise, M. (1996). Mécanismes de corrosion des alliages de zirconium. Etude des cinétiques initiales d'oxydation et du comportement mécanique du système métaloxyde. Dissertation, Ecole Nationale Supérieure des Mines de Paris.

Pilling, N.B. and Bedworth, R.E. (1923). The oxidation of metals at high temperatures. *J. Inst. Metals*, **29**, 529–591.

Roy, C. and Burgess, B. (1970). A study of the stresses generated in zirconia films during the oxidation of zirconium alloys. *Oxidation of Metals*, **2**(3), 235–261.

Sirotine, Y. and Chaskolskaia, M. (1984). *Fondements de la physique des cristaux*. Editions Mir, Moscow.